Eulerian numerical simulation of bubble growth in super-saturated water

by

Yuhang Zhang

A dissertation submitted to The Johns Hopkins University in conformity with the requirements for the degree of Master of Science.

Baltimore, Maryland

November, 2015

Abstract

Occasional super-saturation of river water with dissolved gases downstream of dams and other hydraulic structures is a well-known problem which can lead to large fish mortality up to several kilometres downstream. To explore the possibility and effectiveness of reducing the supersaturation by injecting air bubbles below the water surface, mass exchange process in a dilute liquid-bubble two phase flow is simulated using a computational model in which both time-dependent, three dimensional fluid motion and large numbers of bubbles are calculated in an Eulerian framework. The essay describes the necessary assumptions, its theoretical basis and its ability to simulate realistic length scales. In the analysis of the results, special emphasis is placed on the effects of initial bubble size and depth of bubble injector.

Primary Reader: Prof. Andrea Prosperetti

Secondary Reader: Prof. Rajat Mittal

Contents

CONTENTS

Chapter 1

Introduction

It has been observed that high air super-saturation levels in water can cause gas bubble disease[1] on fishes(see figure 1.1), which leads to high fish mortality rates. Fishes are killed by a mechanism named decompression sickness, also known as "the bends", which is a common danger for deep-sea divers. The excess air enters the fish circulation system, as they pass through the gill and leads to the formation and growth of bubbles. These bubbles can block blood vessels or damage surrounding tissues. Bubble injection proved to be an effective way to reduce gas super-saturation level.[2] The work addressed in this paper is a numerical simulation of bubble growth in super-saturated water, where they are injected into the water body as carriers of oxygen and nitrogen that is removed from the super-saturation solution.

In rivers there are essentially two major mechanisms leading to supersaturation. In the first place, when being released from a dam into a downstream area, water be-

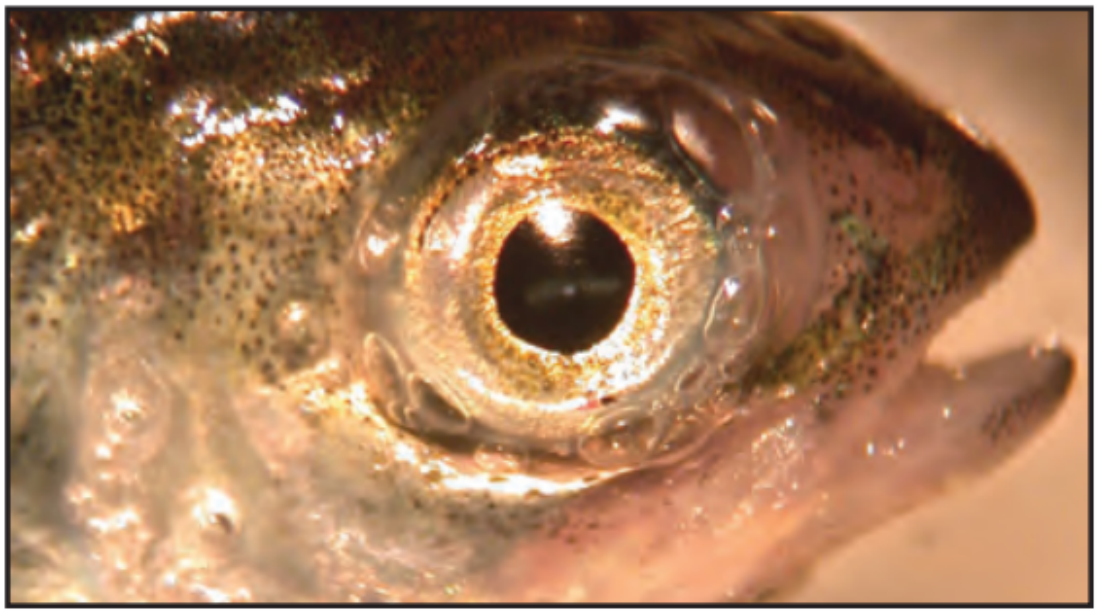

Figure 1.1: Gas bubble disease of fishes: visible gas bubble in vasculature of operculum and in eye as seen in acute gas bubble disease.[3]

comes highly aerated and, when it plunges deeply into the stilling basin, the elevated hydrostatic head forces the air bubbles into solution. Secondly, supersaturation conditions can be established due to the effects of water temperature, which is inversely correlated with gas solubility, and barometric pressure.

Increasing temperature is an obvious way to accelerate the ex-solution of air gases in the water body. But this method turns out to be ineffective because of the very low molecular diffusivity. The time necessary for dissolved gas to diffuse out of the water is too long when facing a big river or water reservoir. The way we propose to deal with this situation is to inject bubbles into the super-saturated solution, thus providing the surfaces for dissolved gas to come out of the solution. Bubbles are removed from the water body after they reach the free surface. Another important effect that comes

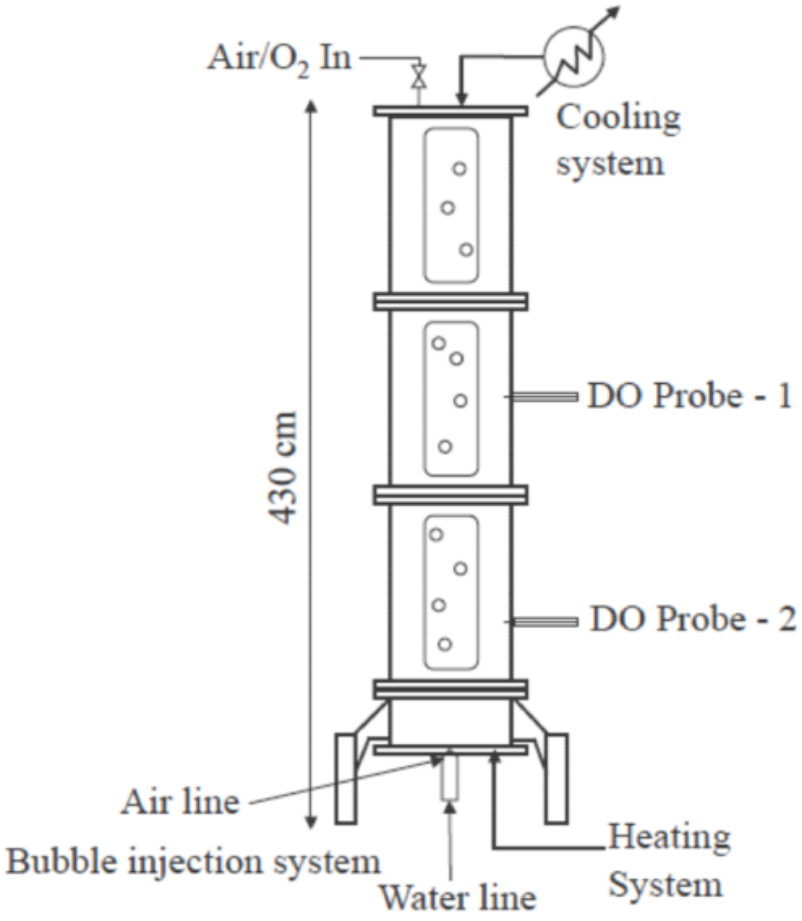

Figure 1.2: Large scale setup of the experimental facility used by Prof. Katz research group to study the air concentration reduction process.[4]

from the bubbles is that their ascensional motion can produce vertical convective currents in the water body thus exposing super-saturated water below the position of the bubble generator.

Experimental work on the air concentration reduction is conducted by another research group in Johns Hopkins university, whose large-scale experimental facility is a water tank(60 cm diameter, 4.3 m high, see figure 1.2) equipped with windows, injection systems, and ports for measuring the dissolved gas content. Super-saturated

liquid is generated by a heating-cooling cycle and injected into the tank from the bottom while monitoring the dissolved gas concentration and bubble size at several elevations. To solve this problem numerically, we want to develop a computational model which is able to simulate momentum and mass exchange process between the bubble and liquid phase. Bubbles are injected into the domain by introducing a source term in the governing equation of bubble phase. By running simulations with different initial conditions, we are able to study how different factor can affect the concentration reduction process.

The efficiency of the process may depend strongly on two factors.

The first one is the bubble size. A given amount of gas distributed in the form of large bubbles is not very effective as the bubbles rise to the surface quickly and do not provide therefore much time for gas to diffuse into them. The same amount of gas injected in the form of smaller bubbles is better insofar as it provides a larger surface area and longer residence time. However, if the bubble radius is too small, the bubbles may either shrink due to the effect of surface tension thus leading to an increase in gas content of the liquid or rise so slowly as to have a negligible effect, especially on promoting convection.

The second important factor is the depth of the bubble generator. Obviously, shallowly generated bubbles leave the water body too quickly thus failing to provide long residence time and strong vertical convective currents. For deeply generated bubbles, initially air gas leaves bubbles and enters water, because in a high pressure

environment the water is still under-saturated. This results in an increase of air concentration, which is definitely contrary to what we intend to achieve. However, for those bubbles which are released in a moderately deep position, with proper initial bubble radii they end up acquiring a long residence time to remove the dissolved gas in the water body, thus ensuring all the bubbles are efficiently utilized.

So in order to achieve a high super-saturation reduction efficiency, a balance between bubble size and bubble generator depth needs to be established. In my work, many numerical simulations with different configurations are run to find a good combination of the two main factors. Multiphase flow numerical simulation is computationally intensive. In order to obtain a shorter simulation time, both the water phase and the bubble phase are treated as fields, in other words, we use an Euler-Euler model to describe this two-phase flow.

Chapter 2

Governing equations of Euler-Euler model

A precise way to model the motion of bubbles would be to establish the motion equation of every single bubble using Newton's second law.[56] But this method requires more computational resources, thus it is really time-consuming when simulating relatively large length scale. Here comes our Euler-Euler model, where bubbles are treated as another continuum, rather than many independent objects. The assumptions behind this model are that the bubble number is sufficiently large and bubble size is so small compared with the length scale we are interested in, thus we only need to resolve the bubble macroscopic motion.

2.1 Bubble number density equation and terminal velocity

The evolution equation for the bubble number density field is

$$\frac{\partial n}{\partial t} + \nabla \cdot (\mathbf{w}n) = 0, \tag{2.1}$$

where $\mathbf{w}$ is the bubble velocity. The bubbles injected to reduce the dissolved air concentration will appear as boundary condition. To find an expression for the bubble velocity field we need to analyse the momentum balance when bubbles are tracked individually, which is

$$\frac{d}{dt}\left(\rho_b v \mathbf{w}\right) = -3\pi f\left(Re_b\right)\mu_w d_b(\mathbf{w}-\mathbf{u}) + \frac{1}{2}\rho_w\left[v\left(\frac{d\mathbf{u}}{dt} - \frac{d\mathbf{w}}{dt}\right) + (\mathbf{u}-\mathbf{w})\frac{dv}{dt}\right] + (\rho_b - \rho_w)v\mathbf{g}, \tag{2.2}$$

where v is the bubble volume, d_b is the bubble diameter, ν_w is the water kinematic viscosity, ρ_w and ρ_b are the density of liquid and bubble respectively, $\mathbf{g}$ is the gravitational acceleration, f is an empirical factor dependent on the bubble Reynolds number

$$f(Re_b) = \begin{cases} 1 + 0.15Re_b^{0.687}, & \text{for} \quad Re_b < 10^3, \\ 0.018Re_b, & \text{for} \quad Re_b > 10^3, \end{cases} \tag{2.3}$$

with $Re_b = d_b|\mathbf{w} - \mathbf{u}|/\nu_w$ the instantaneous Reynolds number of the bubble. This relation was derived for solid spheres but it is, in water, also applicable to bubbles

which tend to be coated with surfactants which immobilize the surface giving rise to a nearly no-slip condition. There are still some other effects that contribute to the total momentum of a bubble, virtual buoyancy, lift and history force, they are so small that it may be neglected in the temporal analysis.

The bubble terminal velocity w_T is obtained when all d/dt terms in the above bubble momentum equation are set to be zero and is

$$w_T = \frac{\rho_w - \rho_b}{\rho_w} \frac{{d_b}^2 |\mathbf{g}|}{18\nu_w f}, \tag{2.4}$$

with f given as above. Note that when f is 1, the expression is the same as the solution given by Sir Stokes for the flow past a solid sphere. For the purpose of simplifying the computation of terminal velocity in each cell, the empirical factor f is set to be 1 in our model. This is the case when bubbles are very small because the strong effect of surface tension keeps them approximately spherical and the rise velocity is small due to the small buoyancy. Very large bubbles are easily broken up upon encountering turbulent eddies or even spontaneously due to instabilities. The terminal velocity of bubbles is a large topic and too complicated to cover it in a few pages. Scientists use some dimensionless groups, Morton number, Eötvös number and Reynolds number, to characterize the shape of bubbles or drops moving in a surrounding fluid phase.[7] Terminal velocity, drag coefficient and bubble shape are influenced by a lot of different effects: surface tension, liquid viscosity, bubble size,

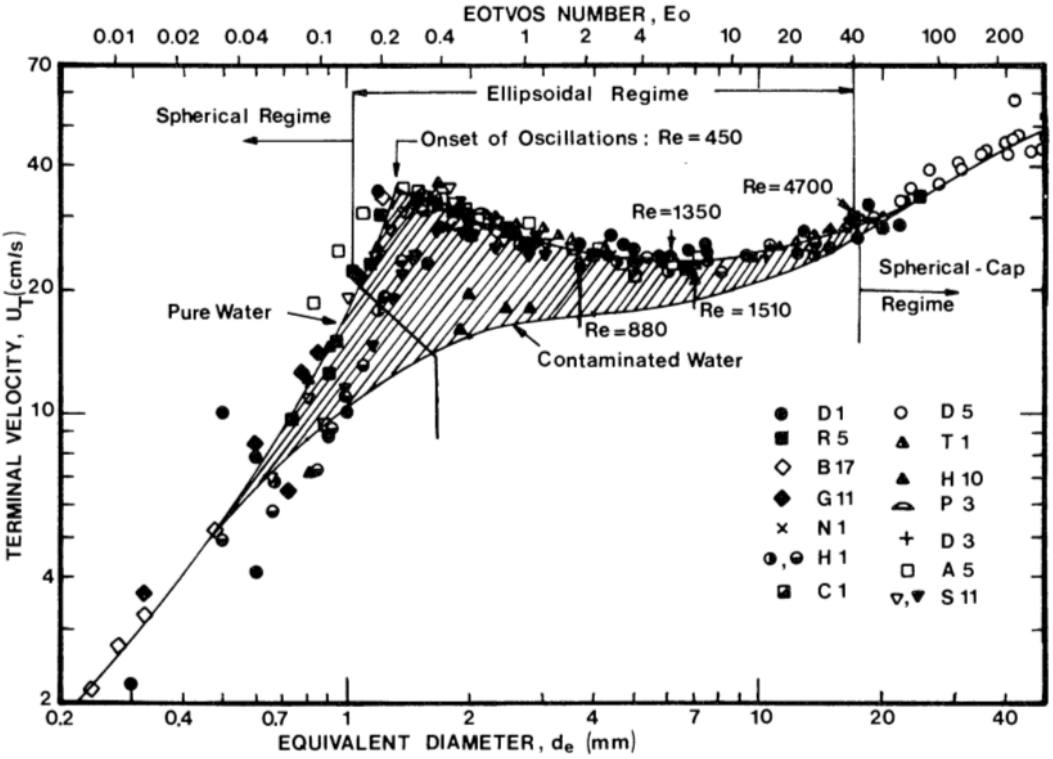

Figure 2.1: Terminal velocity of air bubbles in water at 20 °C.[8] They approximately follow a linear log-log relation given bubble diameter is smaller than 1 mm. Larger bubbles deform ,oscillate and even tend to break up, but their terminal velocities don't exceed a limit value.

liquid contamination, internal circulation. In different shape regimes different effects play dominant roles. Researchers have carried out experiments to find the laws in different circumstances. In order to use a simple model to approximate the former experimental results across many bubble shape regimes, we set a upper limit to it, which is 25 cm/s, avoiding an inauthentic large terminal velocity.

Because bubbles have very little mass, the velocity difference with respect to the surrounding water reaches the terminal velocity very rapidly.[9][10] Then we assume that such transient accelerating process is negligible and terminal velocities are imposed

instantaneously.[11] Thus the bubble velocity field is given by a combination of the local fluid velocity and bubble terminal velocity, as follows

$$\mathbf{w} = \mathbf{u} - w_T \frac{\mathbf{g}}{|\mathbf{g}|}, \tag{2.5}$$

where $\mathbf{u}$ is the liquid velocity at the bubble position and w_T the terminal velocity given above. In the simulations we choose the positive z-axis direction to be opposite to the direction of gravity.

2.2 Mass exchange between bubbles and water

The mass exchange in our case happens between the air inside the bubbles and the dissolved air in the liquid. Two equations are used to describe the mass evolution in the two phases, with source or sink terms representing the mass exchange process.

The mass conservation equation of the bubble phase is

$$\frac{\partial(\rho_b \alpha_b)}{\partial t} + \boldsymbol{\nabla} \cdot (\rho_b \alpha_b \mathbf{w}) = \mathcal{I}, \tag{2.6}$$

where $\alpha_b = n v_b$ is the volume fraction, with n the local number density and v_b the volume of one bubble. $\mathcal{I}$ is the volume source term. In general, it could represent

any type of mass source, chemical reaction or phase change. It includes both the mass exchange between two phases and the mass of bubbles added by the bubble generator. The contribution from bubble injection is explained in the next chapter. The derivation of a specific form of mass exchange source is presented below.

Upon substitution of the volume fraction definition into mass equation (2.5), after expanding the derivatives, we have

$$\frac{\partial(n\rho_b v_b)}{\partial t} + \boldsymbol{\nabla}\cdot(n\rho_b v_b \mathbf{w}) = n\frac{\partial(\rho_b v_b)}{\partial t} + (\rho_b v_b)\frac{\partial n}{\partial t} + n\mathbf{w}\cdot\boldsymbol{\nabla}(\rho_b v_b) + \rho_b v_b \boldsymbol{\nabla}\cdot(n\mathbf{w}) = \mathcal{I}.$$

Upon using the number density equation to simplify this expansion in terms of the material derivative, we have

$$\mathcal{I} = n\frac{D_b}{D_b t}(\rho_b v_b), \tag{2.7}$$

where

$$\frac{D_b}{D_b t} = \frac{\partial}{\partial t} + \mathbf{w}\cdot\boldsymbol{\nabla} \tag{2.8}$$

is the Lagrangian derivative following the bubble phase. Relation (2.6) demonstrates that the total rate of mass exchange between the two phases is equal to the sum of the masses exchanged between each bubble and the liquid, which agrees with the empirical observation. We define the Lagrangian mass transfer rate for a single bubble by

$$\dot{M} = \frac{D_b}{D_b t}(\rho_b v_b) \tag{2.9}$$

to avoid redundant equations in the following discussion. Then the bubble mass conservation equation is written as

$$\frac{\partial(\rho_b \alpha_b)}{\partial t} + \boldsymbol{\nabla} \cdot (\rho_b \alpha_b \mathbf{w}) = n\dot{M}. \tag{2.10}$$

So now we have two equivalent equations describing the same mechanism, namely, the total bubble mass equation and the single bubble mass equation. One of them must be chosen as the one solved numerically. My conclusion is that the total bubble mass equation is a better choice. The reason is explained in the next chapter. So in the numerical simulation we advance total bubble mass equation first, then calculate the bubble diameter, which is needed for the terminal velocity w_T and mass transfer rate $\dot{M}$. To do this we need the bubble density ρ_b, which is a function of water depth. If we assume both atmosphere and the bubbles to be constituted by an ideal gas, then we have

$$\frac{\rho_b}{p_b} = \frac{\rho_{atm}}{p_{atm}}. \tag{2.11}$$

If we assume the pressure inside the bubble is equal to the local hydrostatic pressure, then we have

$$\rho_b = \frac{\rho_{atm}}{p_{atm}}(p_{atm} + \rho g h). \tag{2.12}$$

The transport of the dissolved gas is described by the evolution equation for the concentration field, with the mass transfer rate as a sink. Upon neglecting the very

small volume fraction of the bubbles, the equation is

$$\frac{\partial c}{\partial t} + \boldsymbol{\nabla} \cdot (\mathbf{u}c) = D\boldsymbol{\nabla}^2 c - n\dot{M}, \tag{2.13}$$

where c is the mass concentration, D the diffusivity, $\mathbf{u}$ the fluid velocity, and α_b the volume fraction of the bubbles. The mass transfer rate $\dot{M}$ is given by

$$\dot{M} = \pi d_b^2 h(c - c_{sat}), \tag{2.14}$$

where d_b is the bubble diameter, h is the mass transfer coefficient between liquid and bubbles, $c - c_{sat}$ is the difference between local concentration of the bubble surface and the saturation concentration. The mass transfer coefficient can be calculated from the Sherwood number

$$Sh = \frac{d_b h}{D} = 2 + 0.6 Re^{\frac{1}{2}} Sc^{\frac{1}{3}}, \tag{2.15}$$

in which the Reynolds and Schmidt numbers are

$$Re = \frac{d_b|\mathbf{u} - \mathbf{w}|}{\nu} = \frac{d_b|w_t|}{\nu}, \tag{2.16}$$

$$Sc = \frac{\nu}{D}, \tag{2.17}$$

The saturation concentration at different depths is proportional to pressure, given by

$$c_{sat} = \frac{c_{atm,sat}}{p_{atm}}(p_{atm} + \rho g h), \tag{2.18}$$

where c_{sat} is the saturation concentration at different depth, $c_{atm,sat}$ the saturation concentration at water surface. All the useful physical parameters in our model are listed below in table 2.1.

Table 2.1: Parameter values.

Parameters	Physical Values	Physical Meaning
ρ	$10^3 kg/m^3$	water density
ν	$10^{-6} m^2/s$	water kinematic viscosity
D	$2 \times 10^{-9} m^2/s$	air-water diffusivity
ρ_{atm}	$1.225 kg/m^3$	atmospheric air density
$c_{atm,sat}$	$2.27 \times 10^{-2} kg/m^3$	air solubility in water under atmospheric pressure
g	$9.8 kg \times m/s^2$	gravitational acceleration

2.3 Momentum equation

According to the volume averaged two phase momentum equation for the fluid-bubble mixture we have

$$\frac{\partial}{\partial t}(\rho(1-\alpha_b)\mathbf{u}) + \boldsymbol{\nabla}\cdot(\rho(1-\alpha_b)\mathbf{uu}) + \frac{\partial}{\partial t}(\rho_b\alpha_b\mathbf{w}) + \boldsymbol{\nabla}\cdot(\rho\alpha_b\mathbf{ww}) = \boldsymbol{\nabla}\cdot\boldsymbol{\sigma} + (1-\alpha_b)\rho\mathbf{g} + \alpha_b\rho_b\mathbf{g}, \tag{2.19}$$

where $\mathbf{g}$ is the gravity vector, $\boldsymbol{\sigma}$ the average stress in the mixture, ρ the fluid density, ρ_b the bubble density. Upon considering the liquid continuity equation,

$$\frac{\partial}{\partial t}\left(\rho(1-\alpha_b)\right) + \boldsymbol{\nabla}\cdot\left(\rho(1-\alpha_b)\mathbf{u}\right) = 0, \tag{2.20}$$

the first two terms in the momentum equation (2.19) are simplified to

$$\frac{\partial}{\partial t}\left(\rho(1-\alpha_b)\mathbf{u}\right) + \boldsymbol{\nabla}\cdot\left(\rho(1-\alpha_b)\mathbf{u}\mathbf{u}\right) = \rho(1-\alpha_b)\frac{\partial \mathbf{u}}{\partial t} + \rho(1-\alpha_b)\left(\mathbf{u}\cdot\boldsymbol{\nabla}\right)\mathbf{u}.$$

Upon expanding the next two terms in the momentum equation (2.19) and using the number density equation (2.1), they become

$$\frac{\partial}{\partial t}(\rho_b\alpha_b\mathbf{w}) + \boldsymbol{\nabla}\cdot\left(\rho\alpha_b\mathbf{w}\mathbf{w}\right) = n\left(\frac{\partial}{\partial t}\left(\rho v_b\mathbf{w}\right) + \left(\mathbf{w}\cdot\boldsymbol{\nabla}\right)\left(\rho v_b\mathbf{w}\right)\right) = \frac{D_b}{D_b t}\left(\rho v_b\mathbf{w}\right).$$

Because every bubble is assumed to reach its terminal velocity instantaneously after being released into the water body, all of them are in momentum equilibrium state; in other words, the equation above equals to zero. Upon collecting all four terms on the left-hand side of the mixture momentum equation, we have

$$\rho(1-\alpha_b)\frac{\partial \mathbf{u}}{\partial t} + \rho(1-\alpha_b)\left(\mathbf{u}\cdot\boldsymbol{\nabla}\right)\mathbf{u} = \boldsymbol{\nabla}\cdot\boldsymbol{\sigma} + \rho\mathbf{g} + nv_b(\rho_b-\rho)\mathbf{g}. \tag{2.21}$$

The last term is the force applied by the bubbles on the fluid. In our model, it is assumed that the mass loadings are very small, and the bubble volume fraction can be taken as zero. As a result, we have our final form of the momentum equation, which is

$$\frac{\partial \mathbf{u}}{\partial t} + (\mathbf{u} \cdot \boldsymbol{\nabla})\, \mathbf{u} = \frac{1}{\rho} \boldsymbol{\nabla} \cdot \boldsymbol{\sigma} + \mathbf{g} + n v_b \frac{\rho_b - \rho}{\rho} \mathbf{g}. \tag{2.22}$$

Chapter 3

Equation discretization and numerical implementation

The computational domain is discretized on a regular Cartesian grid with a staggered-grid arrangement. All scalar fields reside on cell centers while all components of vector fields reside on face centers. We numerically solve the equation system fully explicitly. So we use the information from last time step to calculate all the coupling terms between different equations, namely, bubble terminal velocity, mass transfer rate and the force applied by the bubbles on the fluid. Then advance to the next time step. Details are presented below. In this chapter, we use subscripts $i, i+1, i-1$ to denote the cell-centered values, and $i+\frac{1}{2}, i-\frac{1}{2}$ for face-centered values, and $n, n+1, n-1$ for different time step, and i, j, k for three different direction respectively.

3.1 Flow solver

The flow solver used in this code is based on 'Bluebottle' code developed by Mr. Sierakowski.[12] Here only the basic idea of the method is presented. The incompressible Navier-Stokes equation is solved by a second-order in space and time pressure projection method. To proceed from t^n to $t^{n+1} = t^n + \Delta t$, firstly an intermediate velocity is needed

$$\mathbf{u}^* = \mathbf{u} + \Delta t \left[-(\mathbf{u} \cdot \boldsymbol{\nabla}_h \mathbf{u})^{n+1/2} + \nu \left(\boldsymbol{\nabla}_h^2 \mathbf{u} \right)^{1+1/2} \right] \tag{3.1}$$

where the subscript h indicates finite-difference derivatives and the star superscript indicates an intermediate velocity. Then the pressure Poisson problem is solved to enforce continuity equation,

$$\boldsymbol{\nabla}_h^2 p^{n+1/2} = \rho \frac{\boldsymbol{\nabla}_h \cdot \mathbf{u}^*}{\Delta t}. \tag{3.2}$$

The boundary conditions for this pressure field are zero-normal-gradient on all boundaries. The pressure field is used to project intermediate velocity field onto a divergence-free vector space, now we have the velocity field at the next time step,

$$\mathbf{u}^{n+1} = \mathbf{u}^* - \frac{\Delta t}{\rho} \boldsymbol{\nabla}_h p^{n+1/2}. \tag{3.3}$$

3.2 Number density equation and bubble generator

Before calculating the number density equation, we need to know the bubble velocity field **w** at all cell faces, which is equal to the sum of the liquid velocity **u** and bubble terminal velocity $w_T\mathbf{k}$ as shown in (2.4). Because the bubble diameters, which are used to obtain terminal velocities, are located at cell centres, we choose to use upwind bubble diameter values to compute the bubble velocities

$$(w_z)^n_{i+\frac{1}{2},jk} = u^n_{i+\frac{1}{2},jk} + \frac{1}{2}\left[1 - \mathrm{sgn}\left((w_z)^{n-1}_{i+\frac{1}{2},jk}\right)\right](w_T)^n_{i+1,jk} + \frac{1}{2}\left[1 + \mathrm{sgn}\left((w_z)^{n-1}_{i+\frac{1}{2},jk}\right)\right](w_T)^n_{ijk}, \tag{3.4}$$

where $(w_T)^n_{i+1,jk}$ and $(w_T)^n_{ijk}$ are terminal velocities calculated using bubble diameter information at the position.

The number density equation is discretized using a first-order explicit upwind scheme.

$$\frac{n^{n+1}_{ijk} - n^n_{ijk}}{\Delta t} + \frac{(w_x n)^n_{i+\frac{1}{2},jk} - (w_x n)^n_{i-\frac{1}{2},jk}}{\Delta x} + ... = \dot{N}_{source}. \tag{3.5}$$

Here only contribution from x-direction are shown; the ones from other directions are omitted for they have the very same form. The right hand side term $\dot{N}_{source}$ is the volume source of bubble number density, which represents the bubble generator. The bubble generator also appears as a source term $\dot{M}_{source}$ in the bubble mass equation, which is discussed in the next section. w_x is the x-component of bubble velocity.

Note that on our staggered grid, the number density, a scalar field, is a cell-centered value while w_x, w_y, w_z are face-centered. However, $(w_x n)^n_{i+\frac{1}{2},jk}$ as a whole, is the number density flux on one of the two x-direction faces. We use an upwind algorithm to calculate it. In other words, we multiply w_x by a neighbor number density value according to the sign of w_x,

$$n^n_{i+\frac{1}{2},jk} = \frac{1}{2}\left[1 - sgn\left((w_x)^n_{i+\frac{1}{2},jk}\right)\right] n^n_{i+1,jk} + \frac{1}{2}\left[1 + sgn\left((w_x)^n_{i+\frac{1}{2},jk}\right)\right] n^n_{ijk}. \quad (3.6)$$

In an experimental facility, bubbles are typically injected into the water body using a "shower head" with bubble injection ports distributed uniformly on it. To realize a similar bubble injector in a numerical simulation, we add a source term $\dot{N}_{source}$ in the number density equation, which represents the bubble being injected in unit time. A sharp discontinuity of the bubble source field causes instability problem, which leads to the divergence of pressure Poisson equation in the flow solver. To avoid problem, the profile of the source term needs to be smoothed in all three directions to approximate the bubble injector. In the vertical direction, we set the bubble source field to be a Gaussian distribution. In the two horizontal directions, we use hyperbolic tangent functions to smooth the transition from a zero value to some specific bubble

injection rate. Then the number density source term is calculated from

$$\dot{N}_{source} = \dot{N}_* \left(\frac{1}{2}\right)^4 \exp\left(-\frac{(z-z_0)^2}{2\sigma_z^2}\right) \left(1+\tanh\frac{x-L_{x1}}{\epsilon_{x1}}\right) \left(1+\tanh\frac{L_{x2}-x}{\epsilon_{x2}}\right) \cdot \left(1+\tanh\frac{y-L_{y1}}{\epsilon_{y1}}\right) \left(1+\tanh\frac{L_{y2}-y}{\epsilon_{y2}}\right), \quad (3.7)$$

where z_0, L_{x1}, L_{x2}, L_{y1}, L_{y2} are to set up the bubble generator position and size, σ_z, ϵ_{x1}, ϵ_{x2}, ϵ_{y1}, ϵ_{y2} are to configure the smoothness of the bubble source field. The values of these parameters used in the simulations, which is shown in Chapter 4, are listed in table 3.1. The simulation domain is in the form of a rectangular parallelepiped whose horizontal cross section is a square.

Table 3.1: Bubble generator configuration parameters.

Parameters	Dimensionless Values
z_0*	
L_{x1}**	-2.0
L_{x2}**	2.0
L_{y1}***	-2.0
L_{y2}***	2.0
σ_z	0.5
ϵ_{x1}, ϵ_{x2}, ϵ_{y1}, ϵ_{y2}	0.5

*Multiple z_0 values are used to change the bubble generator depth
**$L_{x2} - L_{x1}$ = 50% of x-direction domain size
**$L_{y2} - L_{y1}$ = 50% of y-direction domain size

3.3 Bubble mass equation and concentration equation

The bubble mass equation simulates the mass transfer process between water and bubbles. As for the numerical implementation, there are two equations mathematically which are equivalent to each other because of number density equation. The first one is the total mass equation (2.10), which comes from the basic equation of mass conservation of bubble phase. The second one is the single bubble mass equation (2.9) where Lagrangian manner is used to track a single bubble.

$$\begin{cases} \frac{\partial}{\partial t}(\rho_b \alpha_b) + \boldsymbol{\nabla} \cdot (\rho_b \alpha_b \mathbf{w}) = n\dot{M} \\ \\ \frac{\partial}{\partial t}(\rho_b v_b) + \mathbf{w} \cdot \boldsymbol{\nabla}(\rho_b v_b) = \dot{M} \end{cases}$$

It turns out that the bubble phase total mass equation is a better choice in a numerical simulation. In the early stage of the simulation when most of the domain is empty, because of similarity between the structures of the number density and total mass equations, it can be guaranteed that in all the cells with non-zero number density, the bubble volumes are also non-zero. However for the single bubble equation, this is not true. Ensuring both number density and bubble volume fields advance in the empty domain with the same front shape is important when deciding the positions of non-zero mass exchange rates $\dot{M}$ in the computational procedure. So the total mass

equation is the one we solved in the code. It is discretized as

$$\frac{(nm_b)_{ijk}^{n+1} - (nm_b)_{ijk}^{n}}{\Delta t} + \frac{(w_x nm_b)_{i+\frac{1}{2},jk}^{n} - (w_x nm_b)_{i-\frac{1}{2},jk}^{n}}{\Delta x} + ... = n_{ijk}^{n}(\dot{M})_{ijk}^{n} + (\dot{M}_{source})_{ijk}^{n}, \tag{3.8}$$

where $m_b = \rho_b v_b$ is the mass of bubble, $\dot{M}_{source}$ is the mass source from the bubble generator, which is calculated from

$$(\dot{M}_{source})_{ijk}^{n} = (\rho_b)_{ijk}^{n}(V_b)_{ijk}^{n}(\dot{N}_{source})_{ijk}^{n}, \tag{3.9}$$

where ρ_b is the local bubble density, and V_b the initial bubble volume. ρ_b is different at different depth, and V_b is an initial value given before the start of a simulation. Flux terms are calculated in the same way as in the number density equation. Again the contributions from the other two directions are omitted. The mass transfer rate is

$$(\dot{M})_{ijk}^{n} = \pi(d_{ijk}^{n})^2 h_{ijk}^{n}(c_{ijk}^{n} - c_{sat}), \tag{3.10}$$

where d_{ijk}^{n} is the bubble diameter field, which is calculated from the bubble volume field. c_{sat} is the saturation concentration, which is different at different depth. The mass transfer coefficient h_{ijk}^{n} is given by

$$h_{ijk}^{n} = \frac{D}{d_{ijk}^{n}}(2 + 0.6Re^{1/2}Sc^{1/3}), \tag{3.11}$$

in which

$$Re^n_{ijk} = \frac{d^n_{ijk}|u_{ter}|}{\nu} = \frac{d^n_{ijk}}{\nu}\left|\frac{(d^n_{ijk})^2(\rho-\rho_b)g}{18\mu}\right| \tag{3.12}$$

or

$$h^n_{ijk} = \frac{D}{d^n_{ijk}}\left[2 + 0.6\left(\frac{d^n_{ijk}}{\nu}\left|\frac{(d^n_{ijk})^2(\rho-\rho_b)g}{18\mu}\right|\right)^{1/2}\left(\frac{\nu}{D}\right)^{1/3}\right]. \tag{3.13}$$

Here D is the mass diffusivity of gas in the liquid and μ and ν are the dynamic and kinematic viscosity respectively. The procedure to calculate bubble terminal velocity field is to numerically advance the number density and total mass equations simultaneously, then to divide the total mass by the number density and the bubble density. The result is the bubble volume field, from which we obtain bubble diameter.

For the concentration equation, the advective term is discretized in the same way as the advective term in the number density equation, namely explicitly upwind. The only difference is that the fluid velocity instead of the bubble velocity is used. For the viscous term, we use second order central difference. The source term is given by the number density multiplied by mass transfer rate. For example, the x-direction contribution is

$$\frac{c^{n+1}_{ijk} - c^n_{ijk}}{\Delta t} + \frac{(w_x c)^n_{i+\frac{1}{2},jk} - (w_x c)^n_{i-\frac{1}{2},jk}}{\Delta x} + ... = D\left(\frac{c^n_{i+1,jk} - 2c^n_{ijk} + c^n_{i-1,jk}}{\Delta x^2} + ...\right) - n^n_{ijk}(\dot{M})^n_{ijk}. \tag{3.14}$$

3.4 Computational procedure

Now we are ready to decide the full computational procedure. The first step is to compute the bubble velocity and mass transfer rate. For this purpose, we use both number density field and total bubble mass field nm_b to calculate the bubble diameter field and the terminal velocity, which in turn give the bubble velocity together with the water velocity field. Then we use the bubble diameter field calculated above to compute mass transfer rate. Secondly, with the bubble velocity field and mass transfer rate ready, advance all three equations, number density equation, bubble mass equation and concentration equation, to the next time step. Afterwards, apply boundary conditions on the number density, bubble mass and concentration field. Since the bubble diameter is needed in the coupling term in the momentum equation, this quantity needs to be updated before using the projection method on Navier-Stokes equation. Finally compute the coupling term, i.e. the force applied by the bubble on the water. Then solve the momentum equations. As a result we have the water velocity field at the next time step. The simulation enters a new loop.

3.5 Plane average equation and code testing

In this section we want to verify the correctness of the code under some special configurations. If the mass transfer coefficient is quite small, then the time needed for the bubbles to remove super-saturated concentration will be very long, and since the bubbles don't grow too much, they don't drive a very strong ascensional water motion. In other words, the dominant part of the bubble velocity will be the terminal velocity. Under such assumptions, none of the different fields varies too much along a horizontal direction, so we only need to be interested in the vertical direction. We define quantities averaged over a horizontal plane,

$$\langle(\ldots)\rangle = \frac{1}{S}\int_S (\ldots) dS. \tag{3.15}$$

Then, we assume periodicity boundary conditions in the horizontal directions, and integrate those governing equations. The number density equation becomes

$$\frac{\partial\langle n\rangle}{\partial t} + \frac{\partial\langle w_z n\rangle}{\partial z} = 0. \tag{3.16}$$

To verify the code, we don't use a volume source bubble generator. Instead we set a non-zero Dirichlet boundary condition on the bottom of the domain. Let

$$\langle w_z n \rangle = \langle w_z \rangle \langle n \rangle + (w_z n)'. \tag{3.17}$$

Again, if there are no large variations in horizontal direction, we can assume that the average of multiplication of two values is equal to the multiplication of their averages. Then the second term on the right hand side of the equation above can be discarded, and we have

$$\langle u_{bz} n \rangle \simeq \langle u_{bz} \rangle \langle n \rangle. \tag{3.18}$$

Then the plane-averaged number density equation is

$$\frac{\partial \langle n \rangle}{\partial t} + \frac{\partial}{\partial z} \left(\langle w_z \rangle \langle n \rangle \right) = 0. \tag{3.19}$$

The bubble phase mass conservation equation becomes

$$\frac{\partial}{\partial t}(\langle \rho_b n v_b \rangle) + \frac{\partial}{\partial z}(\langle \rho_b n v_b w_z \rangle) = \langle n \dot{M} \rangle. \tag{3.20}$$

Upon using the same assumptions made earlier, this equation becomes

$$\frac{\partial}{\partial t}(\langle \rho_b \rangle \langle n \rangle \langle v_b \rangle) + \frac{\partial}{\partial z}(\langle \rho_b \rangle \langle n \rangle \langle v_b \rangle \langle w_z \rangle) = \langle n \rangle \langle \dot{M} \rangle. \tag{3.21}$$

The concentration equation is

$$\frac{\partial\langle c\rangle}{\partial t}+\frac{\partial}{\partial z}\left(\langle u_z\rangle\langle c\rangle\right)=D\frac{\partial^2\langle c\rangle}{\partial z^2}-\langle n\rangle\langle\dot{M}\rangle, \tag{3.22}$$

and the z-direction momentum equation

$$\frac{\partial\langle u_z\rangle}{\partial t}+\frac{\partial}{\partial z}\left(\langle u_z\rangle\langle u_z\rangle\right)=\nu\frac{\partial^2\langle u_z\rangle}{\partial z^2}-\langle n\rangle\langle v_b\rangle(\rho-\langle\rho_b\rangle)g. \tag{3.23}$$

In this simulation we have two very important time scales, the time needed for a bubble to leave the water, and the time needed for the concentration to be reduced to the saturation concentration. Under the assumptions we made earlier, the second one is much longer than the first one, so we can assume that the flow reaches a pseudo steady state, which means that the number density and bubble mass profiles in the z direction do not change too much while the the bubbles still need a very long time to absorb all the dissolved gas in the water. Under such assumptions, we eliminate all the time derivatives and take the concentration difference between bubble and water to be a constant. Then we have

$$\frac{\partial}{\partial z}\left(\langle w_z\rangle\langle n\rangle\right)=0 \tag{3.24}$$

and

$$\frac{\partial}{\partial z}(\langle\rho_b\rangle\langle n\rangle\langle v_b\rangle\langle w_z\rangle)=\langle n\rangle\langle\dot{M}\rangle. \tag{3.25}$$

we expand the first term in the left, then divide both side by $\langle n \rangle$, to obtain the simplified result

$$\langle w_z \rangle \frac{\partial}{\partial z}(\langle \rho_b \rangle \langle v_b \rangle) = \langle \dot{M} \rangle. \tag{3.26}$$

At the same time, as stated before, the mass transfer coefficient is too small for the bubbles to significantly change the concentration field, and the dominant part of the bubble velocity is the terminal velocity. So actually we can discard the concentration equation and the momentum equation. The equation (3.26) can be further written as

$$\frac{\partial}{\partial z}\left(\frac{1}{6}\pi \langle d_b \rangle^3 \langle \rho_b \rangle\right) = \frac{1}{\langle d_b \rangle} \frac{18\pi\mu D \Delta c}{(\rho_w - \langle \rho_b \rangle)g} Sh. \tag{3.27}$$

Under the assumption we made earlier, both concentration difference Δc and Sherwood number Sh can be treated as constants. Note that

$$\langle \rho_b \rangle = \rho_b = \rho_{atm}\left(1 + \frac{\rho_w g(H - z)}{p_{atm}}\right), \tag{3.28}$$

where H is the vertical size of the domain. Together with averaged number density equation and the boundary conditions on the bottom for number density n_0 and bubble diameter d_0, we can obtain a number density profile in this pseudo steady state. Then we can compare it with the simulation results with different resolutions. In figure 3.1, the graph shows a good agreement between the profile predicted by plane-averaged equation and the ones from two simulations. At the same time, we

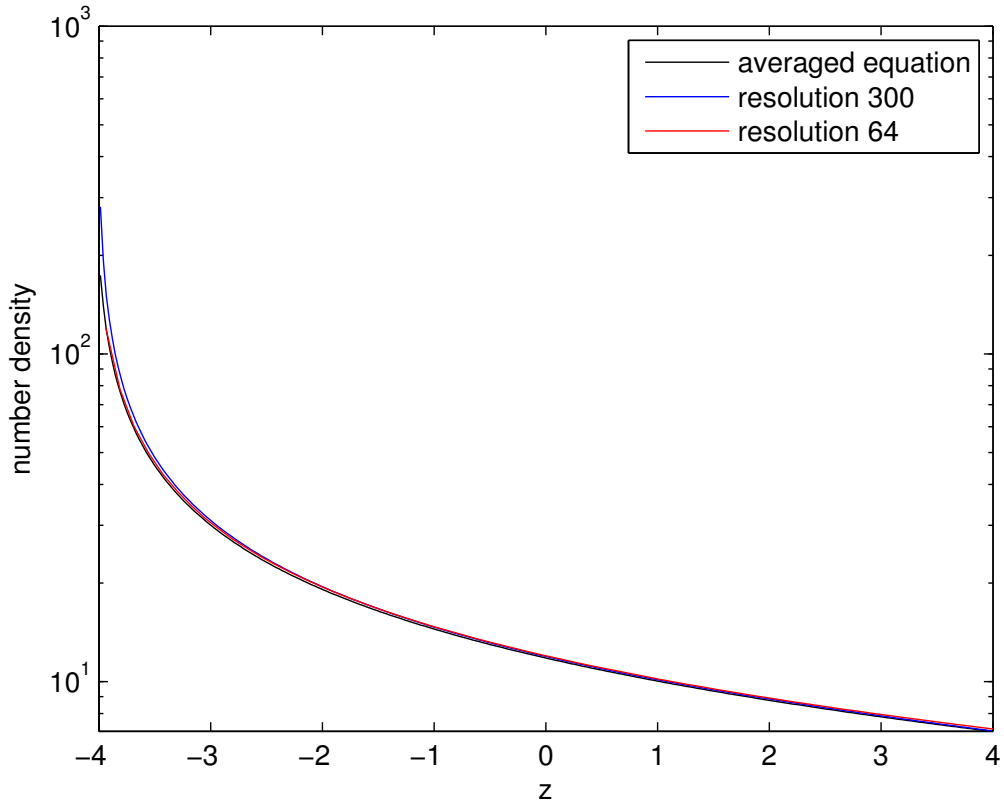

Figure 3.1: This figure shows an agreement between the number density profile predicted by the plane-average equations and the ones from two different resolution computer simulation. z denote the coordinate of vertical direction. All numbers in this figure is dimensionless values.

also show that the results are independent of the grid resolution.

Chapter 4

Numerical results and discussion

A fixed-size water tank in the form of a parallelepiped is adopted in the present work for the simulation of mass exchange process between water and air bubble plumes. The tank is 5 meters high, and has a square cross-section in the horizontal plane, 0.8 meters on each side. By initializing the bubble injector in the middle area of the tank, we are able to study how the bubbles being injected affect the air concentration both above and below the injector position. In our simulations, instead of being injected uniformly across the whole horizontal plane, bubbles are generated only in the central area of it. So there are gaps between the lateral domain boundary and the bubble generator.

For the fluid velocity field, the boundary condition on top is free-slip, and the bottom is set to be a non-slip wall. On all other four lateral domain boundaries, periodicity boundary conditions are used. These four boundaries are periodic also for

the number density field, air concentration and bubble mass. We use zero Neumann boundary conditions for these three fields on both top and bottom boundaries. In other words, there are no diffusive fluxes out of the domain. Because the number density and bubble mass evolve by the bubble velocity, which is the sum of fluid velocity and bubble terminal velocity as mentioned in chapter 2, there exist negative convective fluxes for them on the top boundary. So bubbles enter the simulation domain through the bubble generator, and leave through the top boundary.

Two groups of simulations have been run to study how the initial bubble diameter or bubble generator depth affect the efficiency of the concentration reduction process. For both groups, the initial air gas concentrations are uniformly 30 percent higher than the saturation value at water surface. In the first group of simulations, bubbles are injected at different depths ranging from 2.2 to 4.6 m, while keeping all other parameters the same, including initial bubble diameter, which is 100 μm, and injection volume rates, about 5.23 ml per second. The duration of the simulation is 500 seconds. In the second group of simulations, to study the effect of bubble diameter, with the position of bubbler and total volume injection rate being constant, many cases with different initial bubble diameters are simulated, from 100 μm up to 1 mm. The bubble volume rate used in this group of simulations is higher than in the first one, namely 26.15 ml/s. The total simulation duration here is 100 seconds.

The whole domain is partitioned into $80\times80\times500$ cubic cells for all the simulations. The time step is decided based on stability criteria for both convection and diffusion

terms in all the equations mentioned earlier. Using these parameter sets, stable numerical solutions are achieved with different initial configurations.

4.1 The effect of bubble generator depth

Figure 4.1 shows the number density profiles, volume fraction fields, concentration contours of dissolved air gas and bubble diameters in two of the seven simulations. As shown in these figures, bubbles rise from the central area of the domain because of buoyancy, inducing an upward flow of water above the bubble generator position. This effect drives a circulation inside the water tank: water rises near the bubble plume and falls down near the lateral boundary. Driven by this circulation, the still water containing large amount of dissolved gas below the bubble generator moves up to a higher area, where the local saturation concentration is lower and the dissolved gas can leave the water.

An important observation is that this circulation can only significantly affect a limited area below the position where bubbles are injected. The dilemma we are facing is that we want to induce a strong circulation inside the domain as deep as we can to disturb the whole water body and thus reduce the dissolved gas concentration. But the saturation point is higher in the deeper area because of higher hydrostatic pressure. As a result, with the same amount of dissolved gas, the water gas solution in a deeper area is under-saturated and thus can absorb the air in the bubbles being

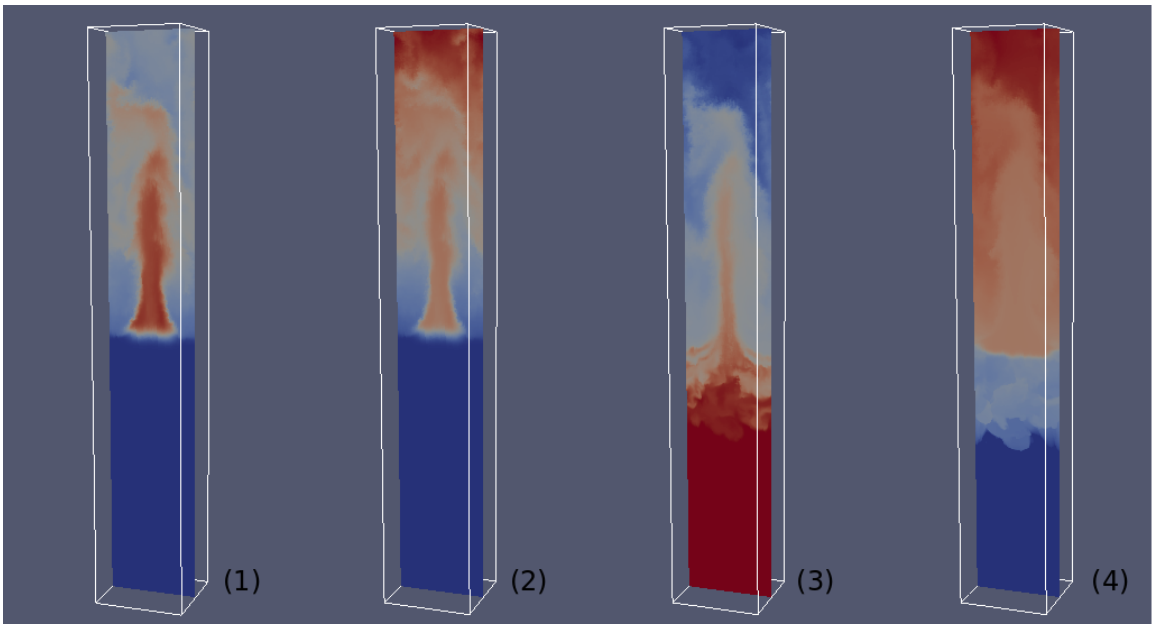

(a) Bubbler depth 2.6 m. (1)bubble number density: $0 \sim 2.3 \times 10^9 m^{-3}$, (2)bubble phase volume fraction: $0 \sim 0.17$ %, (3)air gas concentration: $2.45 \times 10^{-2} \sim 2.951 \times 10^{-2} kg/m^3$, (4)bubble diameter: $0 \sim 150$ μm.

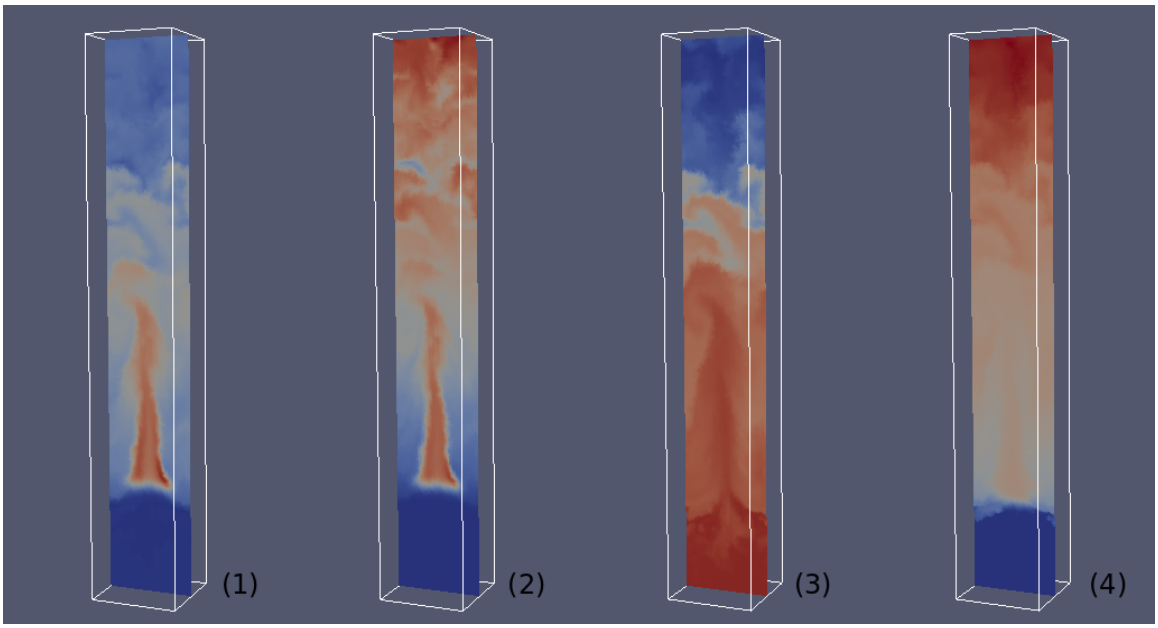

(b) Bubbler depth 4.0 m. (1)bubble number density: $0 \sim 2.85 \times 10^9 m^{-3}$, (2)bubble phase volume fraction: $0 \sim 0.14$ %, (3)air gas concentration: $2.5 \times 10^{-2} \sim 2.951 \times 10^{-2} kg/m^3$, (4)bubble diameter: $0 \sim 170$ μm.

Figure 4.1: The effect of bubble generator depth on the concentration reduction process. Snapshots of central plane from two different simulations at t = 500s are shown here with bubbler parameters: 100 μm initial bubble diameter, 5.23 ml/s injection volume rate.

injected. In other words, bubbles cannot be injected too deeply into the domain.

In our cases the initial concentration value uniformly equals to 130% of the saturation at water surface, so near a depth of 3 m the initial concentration value is equal to the local saturation point. Above this depth, water is super-saturated, but below it, it is under-saturated. If the bubbles are injected deeper than this depth, the air concentration will be increased initially before being reduced. As shown in figure 4.2, because of this effect, even though a larger circulation is generated inside the domain, the dissolved gas concentration below 3 meters cannot be significantly reduced, thus diminishing the total dissolved gas reduction efficiency. Clearly injecting bubbles in about 3 meter deep area is a preferable solution. By doing so, a large circulation is induced to bring up the water in the deep area while avoiding the air to be transferred in the wrong direction. Figure 4.3 shows the concentration averages across the whole domain as a function of time for all the simulations with different initial bubble generator depths in the first simulation group. For those cases in which bubbles are injected into the domain deeper than 3 meters, the concentrations are increased by some amount in the early stage of the simulations. As simulations go on, too shallow or deep bubbler lose their potential to reduce air gas concentration due to either smaller circulation or counterproductive mass transfer direction.

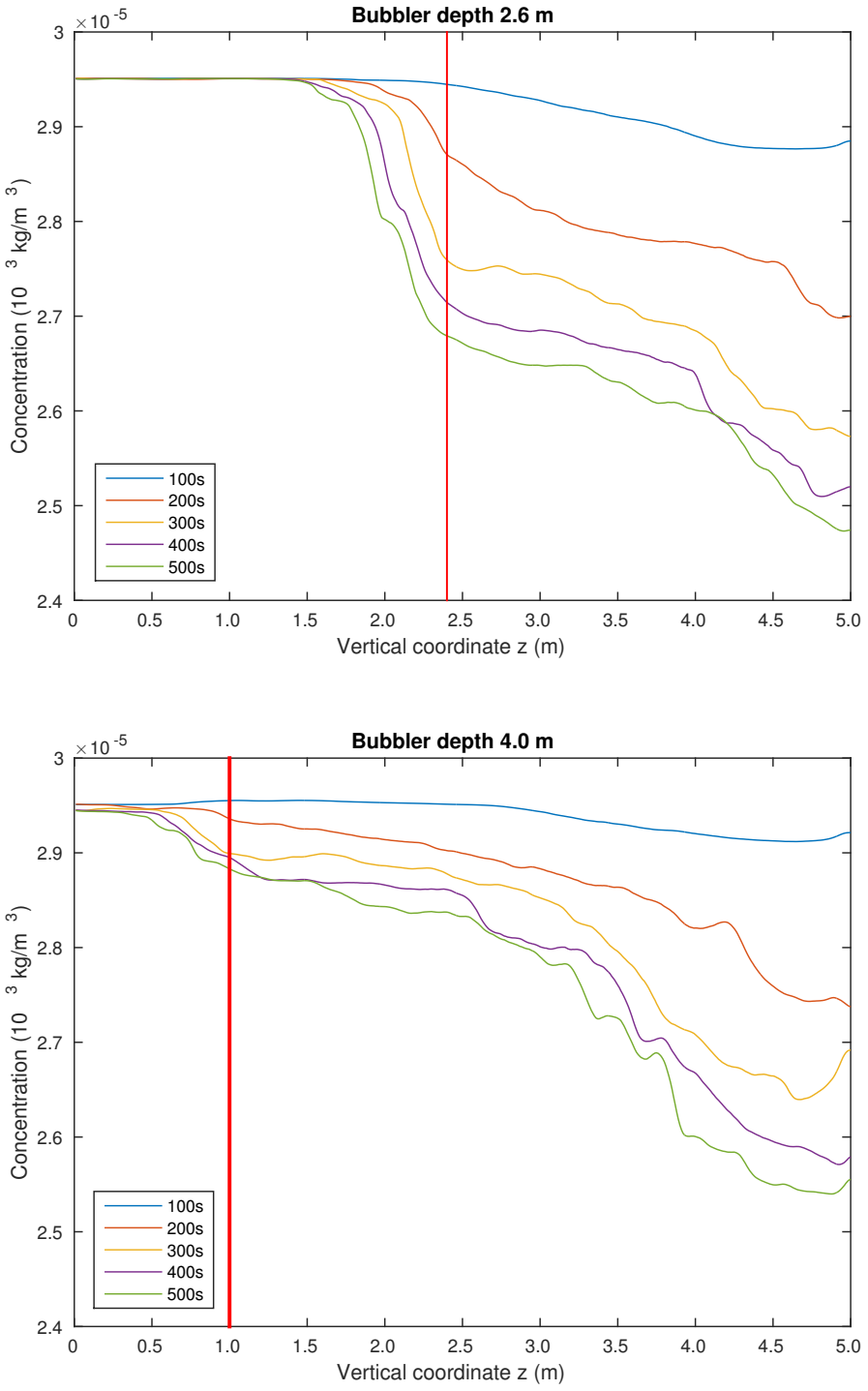

Figure 4.2: Horizontal-plane-averaged air concentration in the water body of two cases as a function of vertical distance at different time steps; the vertical red solid line is the position of the bubble generator.

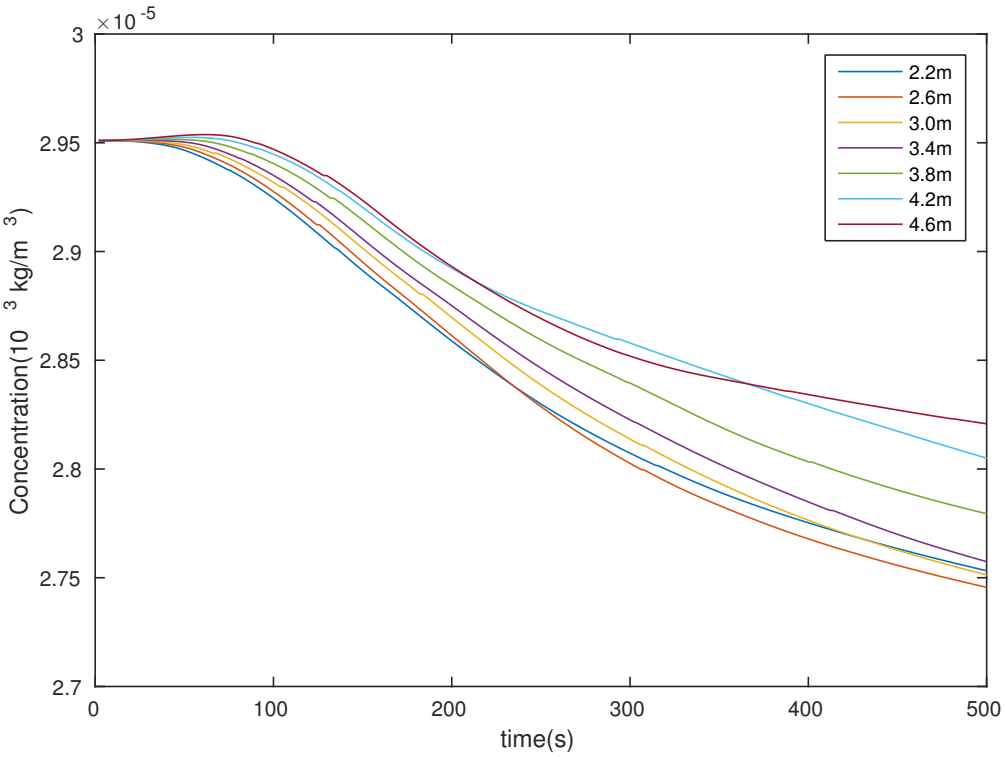

Figure 4.3: Whole domain concentration average as a function of time for different simulations with bubbles being injected at different depth while keeping other parameters the same.

4.2 The effect of initial bubble diameter

With a constant total volume of bubbles being injected in unit time, the contact surface area between bubbles and water is decided by the bubble size. Given the same initial concentration fields, we have the largest mass exchange rate between two phases for the smallest bubbles.

As shown in figure 4.4, at t = 50 s, the air concentrations are in an ascending order of initial bubble diameter in all different depths. In other words, given a constant total bubble injection volume, more concentration is reduced when smaller size bubbles are

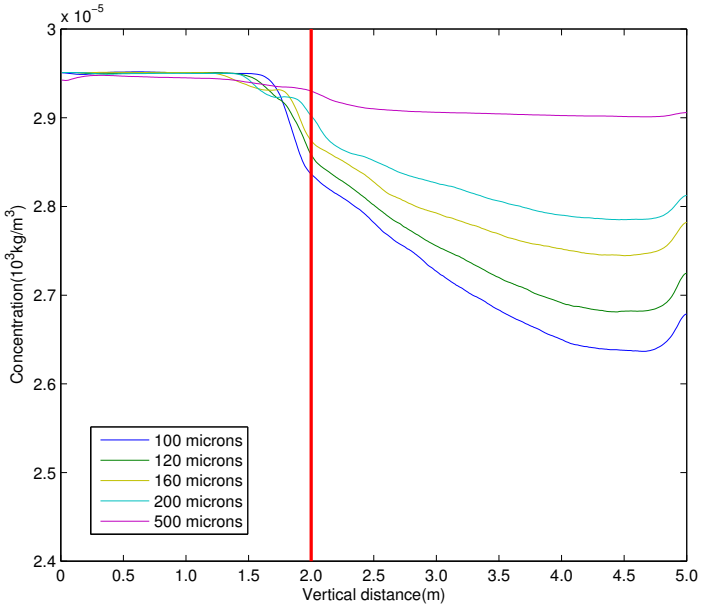

(a) t = 50s

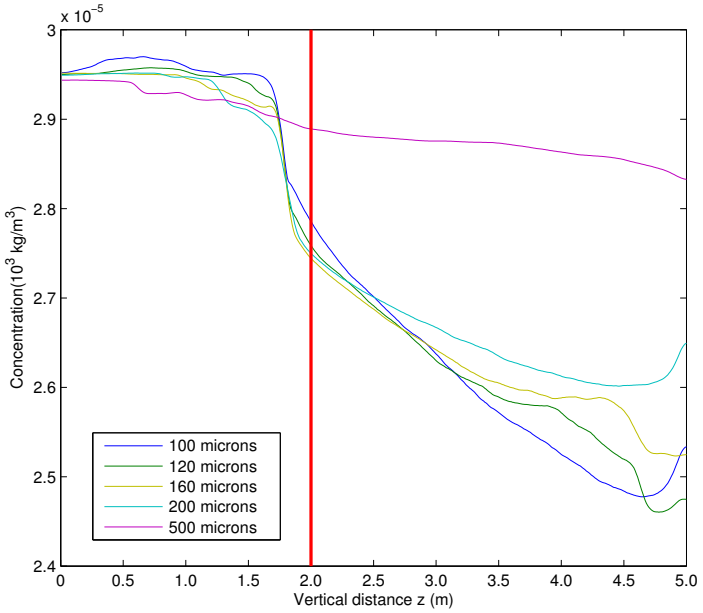

(b) t = 100s

Figure 4.4: Horizontal-plane-averaged air concentration in the domain as a function of vertical distance for 5 simulations with different initial bubble sizes at two time levels. The figures shown here are, respectively, (a) at t = 50s, (b) at t = 100s; the red vertical lines mark the position of bubble generator.

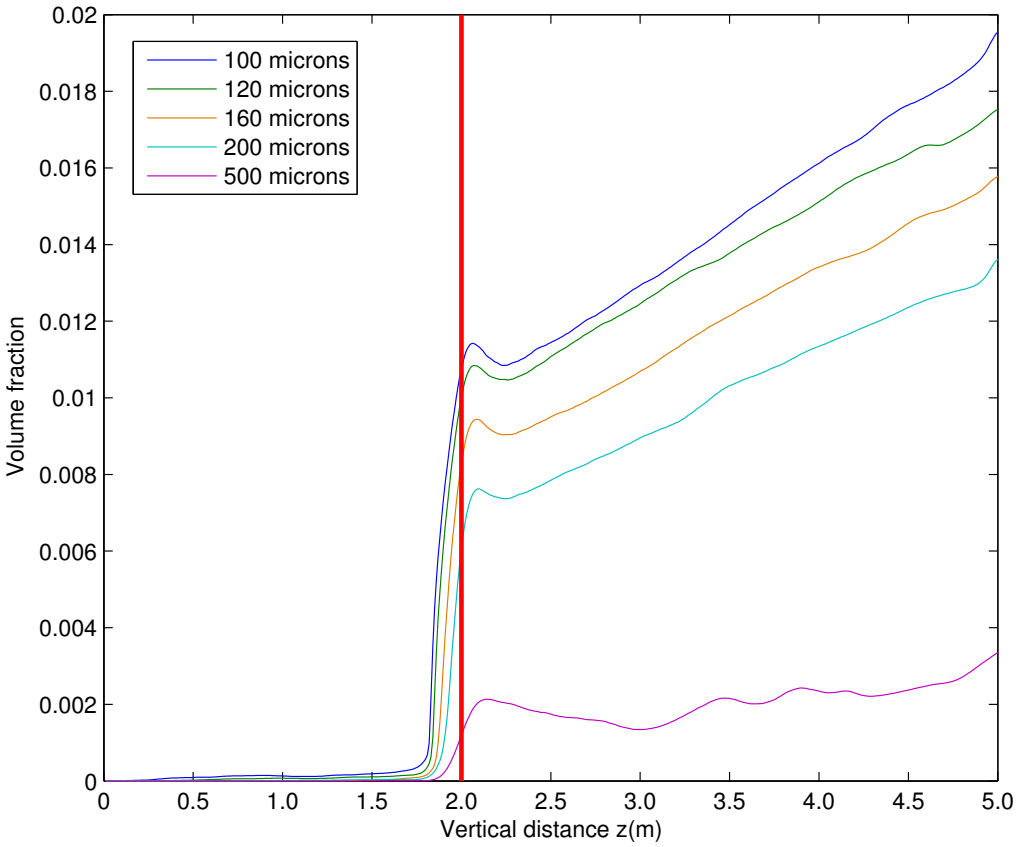

Figure 4.5: Plane-averaged volume fraction as a function of vertical distance z for 5 simulations with different initial bubble diameters at t = 100s; the red vertical solid line is where the bubbles are injected.

injected. And at t = 100 s, due to a larger bubble volume injection rate with respect to the simulations in the first group, in some cases with smaller initial bubble size, such as bubble diameter equals to 100 or 120 μm, the concentrations are almost reduced to the local saturation concentration. The volume fraction distribution in the z direction in these cases are presented in figure 4.5. Because of the fastest mass exchange rate in the case 100 μm bubble diameter, the highest volume fraction occurs in this case, and

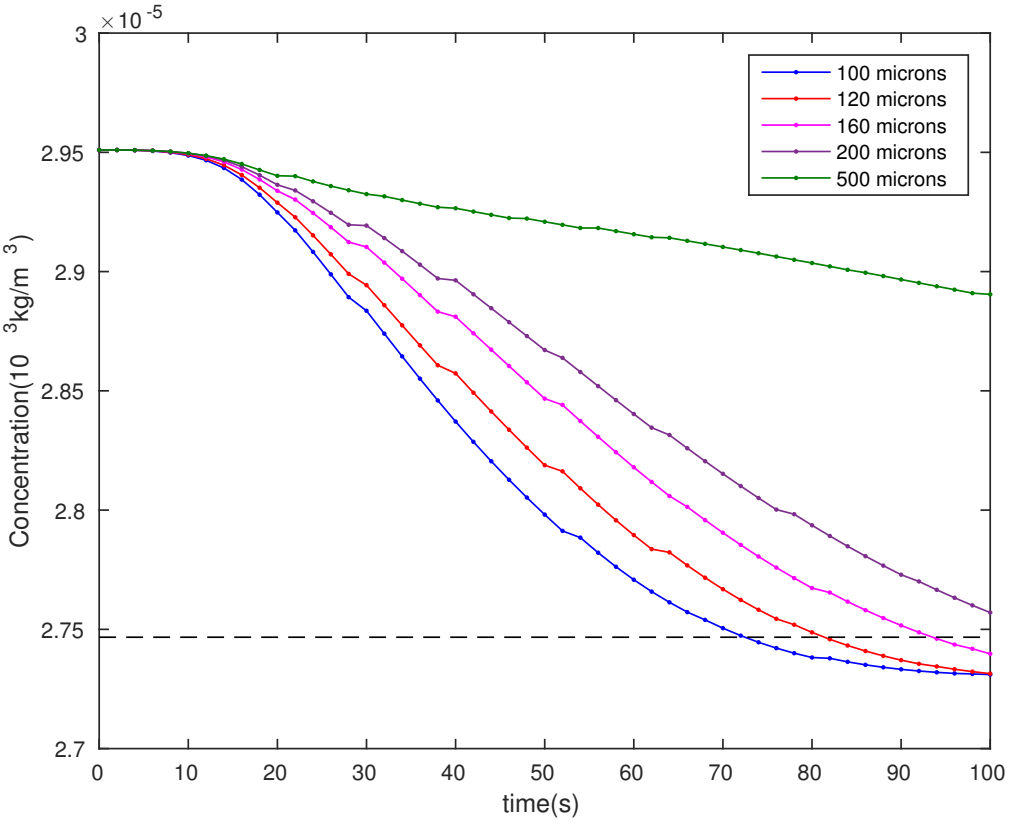

Figure 4.6: Whole domain concentration average as a function of time for different simulations with bubbles being injected at the same position but with different initial bubble sizes; the horizontal black dashed line marks the concentration value assuming all the fluids above the bubble generator are saturated while other fluids below still contain the initial uniform concentration.

is around 2 percent. In both figures 4.4 and 4.5, the performance of 500 μm bubble are much worse than other simulations because of the much larger initial size. Figure 4.6 shows the evolution of the average concentration over the whole domain. We can see that the concentration reduction processes tend to slow down near the end of the simulations for the blue, red and pink lines because most of the supersaturation has been absorbed by the bubbles and leave the domain. An estimated value is

calculated assuming all the fluids above the bubble generator position reach their saturation point while the remaining water below still contains the initial uniform concentration. This value is marked in figure 4.6 by a dashed horizontal line. We find that most of the curves, except for 500 μm bubbles, already cross or tend to cross this line. The reason is that some dissolved air in the water below the bubble generator, even though only a small amount, can be affected by the vertical convective current generated by the bubbles injected above.

Bibliography

[1] D. Weitkamp, "A review of dissolved gas supersaturation literature," *Transactions of the American Fisheries Society*, vol. 109, no. 6, pp. 659–702, NOVEMBER 1980.

[2] A. Prosperetti and X. Geng, "Study of the effectiveness of a laboratory scale system to reduce water super-saturation," Department of Mechnical Engineering, The Johns Hopkins University, Baltimore, MD, 21218, U.S.A, Tech. Rep., APRIL 2006, to the U.S. Bureau of Reclamation, Water Treatment Engineering and Research.

[3] Gas bubble disease. [Online]. Available: https://www.adfg.alaska.gov/static/species/disease/pdfs/fishdiseases/gas_bubble_disease.pdf

[4] A. Prosperetti and J. Katz, "Study of the effectiveness of a laboratory scale system to reduce water super-saturation," Department of Mechnical Engineering, The Johns Hopkins University, Baltimore, MD, 21218, U.S.A, Tech. Rep., MARCH 2015, progress report to the U.S. Bureau of Reclamation.

BIBLIOGRAPHY

[5] J. K.Eaton, "Two-way coupled turbulence simulations of gas-particle flows," *International Journal of Multiphase Flow*, vol. 35, pp. 792–800, 2009.

[6] P. Oresta, F. Fornarelli, and A. Proeperetti, "Multiphase rayleigh-bnard convection," *Mechanical Engineering Reviews*, vol. 1, no. 1-18, pp. 624–642, JANUARY 2014.

[7] T. Maxworthy, C. Gnann, M. Kurten, and F. Durst, "Experiments on the rise of air bubbles in clean viscous liquids," *J. Fluid Mech.*, vol. 321, pp. 421–441, 1996.

[8] M. E. Weber, R. Clift, and J. R. G. and, "Bubbles, drops, and particles." New York, San Francisco, London: Academic Press, 1978.

[9] Y. ZHANG and J. A. FINCH, "A note on single bubble motion in surfactant solutions," *J. Fluid Mech.*, vol. 429, pp. 63–66, 2001.

[10] X. Gong, S. Takagi, and Y. Matsumoto, "The effect of bubble-induced liquid flow on mass transfer in bubble plumes," *International Journal of Multiphase Flow*, vol. 35, pp. 155–162, 2009.

[11] F. Necker, C.Hartel, L.Kleiser, and E.Meiburg, "High-resolution simulations of particle-driven gravity currents," *International Journal of Multiphase Flow*, vol. 28, pp. 279–300, 2002.

BIBLIOGRAPHY

[12] A. Sierakowski. Bluebottle wiki. [Online]. Available: http://lucan.me.jhu.edu/wiki/index.php/Bluebottle

Vita

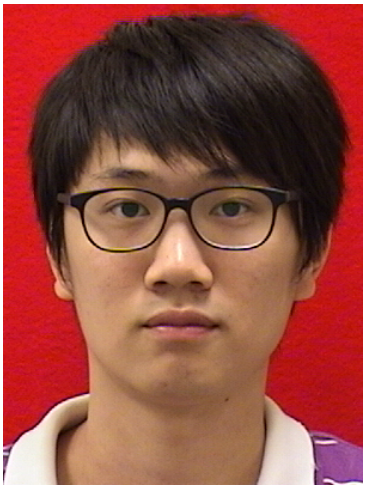

Yuhang Zhang received the Bachelor of Science degree in Theoretical and Applied Mechanics from Sun Yat-sen University in 2013, and enrolled in the Mechanical Engineering M.S.E. program at Johns Hopkins University in 2013. He won the Sun Yat-sen University National Scholarship in 2011, and received a Johns Hopkins University Departmental Payback Fellowship in 2015. His research focuses on computational fluid dynamics and multiphase flow.